Structural properties of invasion percolation with and without trapping: Shortest path and distributions

Stefan Schwarzer,[1,2] Shlomo Havlin,[2] and Armin Bunde[3]
[1]*Institut für Computeranwendungen 1, Universität Stuttgart, 70569 Stuttgart, Germany*
[2]*Minerva Center and Department of Physics, Bar-Ilan University, 52900 Ramat Gan, Israel*
[3]*Institut für Theoretische Physik III, Universität Gießen, Heinrich-Buff-Ring 16, 35392 Gießen, Germany*
(Received 23 October 1997; revised manuscript received 20 November 1998)

We study several structural properties including the shortest path l between two sites separated by a Euclidean distance r of invasion percolation with trapping (TIP) and without trapping (NIP). For the trapping case we find that the mass M scales with l as $M \sim l^{d_l}$ with $d_l = 1.510 \pm 0.005$ and l scales with r as $l \sim r^{d_{\min}}$ with $d_{\min} = 1.213 \pm 0.005$, whereas in the nontrapping case $d_l = 1.671 \pm 0.006$ and $d_{\min} = 1.133 \pm 0.005$. These values further support previous results that NIP and TIP are in distinct universality classes. We also study numerically using scaling approaches the distribution $N(l,r)$ of the lengths of the shortest paths connecting two sites at distance r in NIP and TIP. We find that it obeys a scaling form $N(l,r) \sim r^{d_f - 1 - d_{\min}} f(l/r^{d_{\min}})$. The scaling function has a power-law tail for large x values, $f(x) \sim x^{-h}$, with a universal value of $h \approx 2$ for both models within our numerical accuracy. [S1063-651X(99)12603-5]

PACS number(s): 61.43.Hv, 05.60.−k, 82.20.Wt

I. INTRODUCTION

Invasion percolation has been introduced by Wilkinson and Willemsen [1] as a model to describe the evolution of the front between two immiscible liquids in a random medium when one liquid is displaced by injection of the other. This process occurs, for example, when water is injected into oil reservoirs in order to produce oil. Two model variants have been proposed. The first, nontrapping invasion percolation (NIP), applies for compressible liquids in which the invading liquid always enters the largest available pore on the replaced side of the advancing front. The other, invasion percolation with trapping (TIP), finds application for incompressible liquids where the invasion of a pore is forbidden by the incompressibility constraint when the replaced liquid is completely surrounded by the intruder—this variant is called invasion percolation with trapping. Apart from the possible applications, interest in the NIP and TIP models arises because both are parameter-free models and self-organize into critical states [2,3].

In two dimensions (2D) as well as in three dimensions (3D), numerical studies of NIP and convincing heuristic arguments indicate that NIP falls into the same universality class as regular percolation [1]. This finding is believed to hold for all dimensions.

The situation for TIP is more complicated. Numerical studies have found that the fractal dimension d_f in 2D of the NIP ($d_f \approx 1.90$) and TIP ($d_f \approx 1.82$) [4–6] models differs only by about 4%. This difference is small and heuristic arguments suggest that in three and higher dimensions the trapping becomes irrelevant so that NIP and TIP are in the same universality class. Only recently it has been argued [7], using a mapping from optimal paths to shortest paths, that at least in three dimensions TIP is in a different universality class from that of regular percolation. Earlier numerical results for the fractal dimension of the clusters had suggested that NIP and TIP in 3D fall into the same universality class as regular percolation [1].

Therefore, the possibility that finite-size or crossover effects are responsible for the difference (in 2D) or the agreement (in 3D) of the cluster fractal dimensions cannot *a priori* be excluded. Furthermore, there exist only heuristic but no rigorous arguments that NIP falls into the universality class of regular percolation, i.e., that d_f exactly equals 91/48. To test these questions, we believe that it is important to search for properties in which the two models differ more significantly than in the fractal dimension, and at the same time to collect more evidence that two-dimensional (2D) NIP falls into the regular percolation class.

In this paper we study, apart from the fractal dimension (Sec. II B), several other structural properties of NIP and TIP. Among those are the length l of the shortest path (also called chemical distance) connecting two sites of a cluster at Euclidean distance r (Sec. III B) and the cluster mass $M(l)$ contained within a chemical distance l from a given site (Sec. III). The chemical distance is useful to understand transport properties in disordered media [8].

As an applied example let us mention the problem of oil recovery, where water or steam is injected into one borehole in order to recover oil from another. Here, the chemical distance between the two boreholes is directly related to the time of breakthrough of the injected medium at the second hole [9].

We also study the distribution $N(l,r)$ of the number of cluster sites with chemical distance l and Euclidean distance r from the cluster center. This distribution has been studied in a variety of contexts (see, e.g., [8]). For example, for self-avoiding walk (SAW) chains, it provides insight into dynamical properties such as the propagation of excitations along the chain which can perform ''jumps'' at the positions where chain elements come close. De Gennes conjectured the form of this distribution for SAW [10]. Since his arguments possibly apply in a broader context [11], we test numerically their validity in the NIP and TIP cases (Sec. IV). We find there a scaling form of $N(l,r) \sim r^{d_f - 1 - d_{\min}} f(l/r^{d_{\min}})$, with

the property that $f(x) \sim x^{-h}$ with $h \simeq 2$ for large x, *independent* of the model (NIP or TIP).

From the scaling form of $N(l,r)$ we then compute the average value of $\langle l(r) \rangle$ for fixed values of r, e.g., close to the origin $r=0$. The value of $h=2$ causes the divergence with system size of all moments of l greater than or equal to 1 (Sec. IV C). We conclude and summarize our results in Sec. V.

II. STRUCTURAL PROPERTIES

A. The models

To generate invasion percolation clusters (NIP) in 2D, we perform the following steps. (i) We first assign random numbers on a 2D square array of size $L \times L$. Then (ii) we initiate the growth by occupying the center site of the lattice (start the injection of water into the oil reservoir). In step (iii) we search along the perimeter of the cluster for the site with the largest random number (corresponding to the largest pore). This perimeter site is then (iv) added to the aggregate (replacing the oil in the pore by water). The last two steps (iii) and (iv) are then repeated to grow larger and larger clusters [12].

In TIP one checks at each step of the growth process whether the occupied site has closed a loop (trapped replaced liquid). The rules are such that liquid cannot escape through necks created by next-nearest-neighbor occupied sites on the lattice. The liquid can escape only through a free path at least one lattice unit wide. If a loop has been closed, then we forbid the invasion on all enclosed internal perimeter sites of the aggregate, i.e., we restrict the search of the next largest random number to only the external perimeter sites of the cluster [13].

B. Fractal dimensions

We grow the clusters in steps, stopping at logarithmically spaced cluster masses of up to $M=500\,000$. In Fig. 1 we show two typical clusters of the two invasion percolation models of mass $M=50\,000$. It is apparent from the figure that TIP has larger trapped regions on all scales, therefore suggesting a smaller fractal dimension d_f than NIP.

To obtain the fractal dimension quantitatively, we measure the radius of gyration r_g of the clusters versus their mass M and display the results in Fig. 2(a) for NIP and TIP. For both models we average data from two enembles, one with 25 000 and 50 000 clusters of masses $\leqslant 40\,000$, the other with ≈ 5000 clusters of mass $\leqslant 500\,000$. For algorithmic reasons the cluster growth has been terminated at span $L=3300$. Although we have chosen the largest feasible values of L, we could not avoid a slight finite-size effect in the data point corresponding to the largest mass: a fraction of about 0.01 of all the generated clusters have had a span too large to fit on the simulation array. The average span is approximately 2450. Since the missing configurations are very elongated, r_g is rendered slightly too small at $M=500\,000$. However, we find that this bias is well within the statistical error of our data.

In Fig. 2(a) we do not plot r_g directly, but the rescaled value $r_g/M^{1/d_f}$, which asymptotically approaches a constant value. A horizontal line is plotted for comparison. The plot is quite sensitive to the correct value of d_f, which we have obtained by consideration of the local fractal dimensions $d_f(M) \equiv \Delta \ln M / \Delta \ln r_g$. These values converge to the fractal dimension d_f of the clusters in the limit $M \to \infty$. Finite-size scaling suggests that $|d_f - d_f(M)| \sim M^{-a}$, where a is an *a priori* unknown model-dependent correction-to-scaling exponent [14,15]. Demanding that $d_f - d_f(M)$ vs M^{-a} should be linear for large M, we estimate values of $a=0.80 \pm 0.15$ for NIP and 0.60 ± 0.15 for TIP and obtain the corresponding plots in Fig. 2(b). A straight line fit to the data in the displayed range intersects the abscissa at d_f.

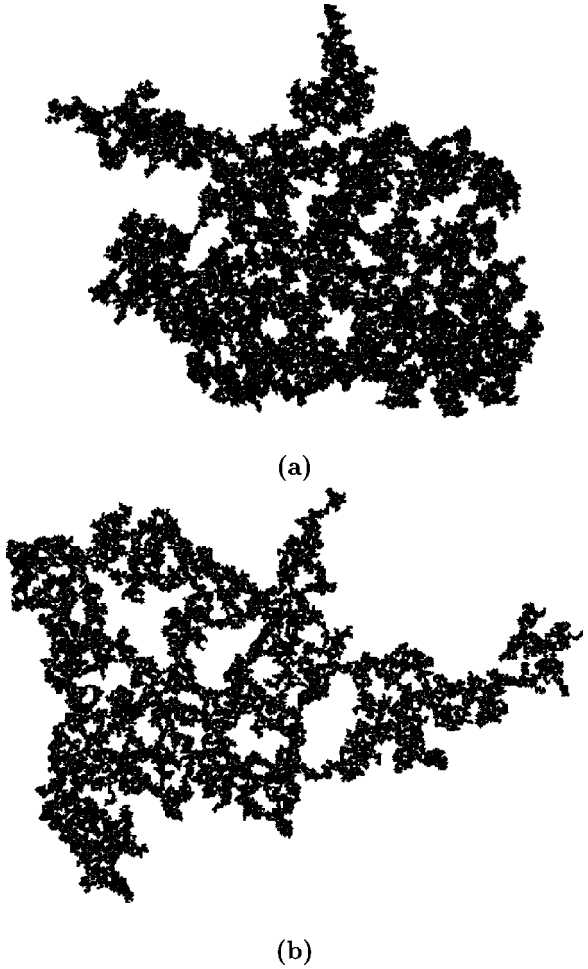

FIG. 1. Snapshots of a NIP (a) and a TIP (b) cluster of mass $M=50\,000$.

We obtain intersections at $d_f = 1.899 \pm 0.003$ for NIP and $d_f = 1.831 \pm 0.003$ for TIP. The measured fractal dimension of NIP is in very good agreement with the exact value $91/48 \approx 1.896$ of regular 2D percolation [16]. The dimension of TIP is larger than the value 1.82 often found in the literature [5,6], but is also more precise. The fractal dimensions of NIP and TIP differ by about 20 standard deviations and thus we confirm that in 2D the two models belong to different universality classes.

III. CHEMICAL DISTANCE

A. Total mass

Next we study the chemical distance in the generated clusters. To this end, we consider the cluster connectivity at

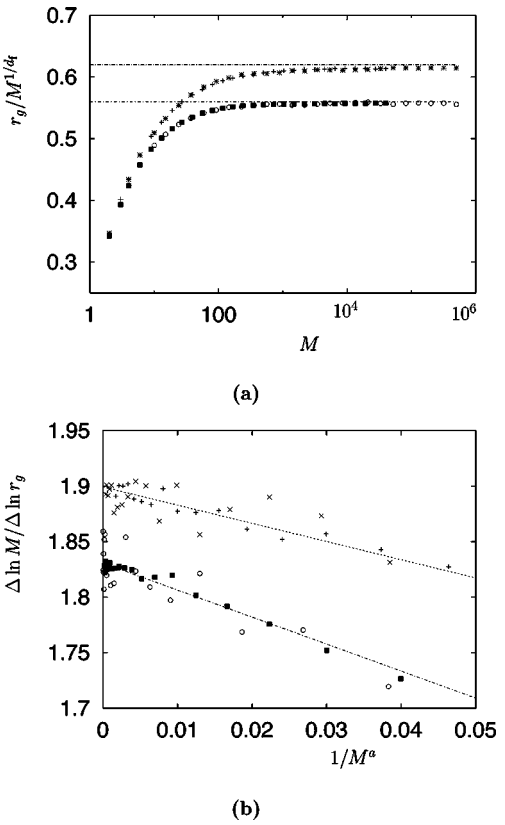

FIG. 2. (a) Plot of the radius of gyration r_g divided by M^{1/d_f} with $d_f=1.899$ (NIP) and $d_f=1.831$ (TIP) vs the number of sites M in the cluster. For NIP we have averaged over 25 000 systems of mass $M\leqslant 40\,000$ (+) and 5050 systems of $M\leqslant 500\,000$ (*) and for TIP over 50 000 systems of $M\leqslant 40\,000$ (■) and 5750 systems of mass $M=500\,000$ (○). For large M, the graphs become horizontal, indicating that the fractal dimensions equal the chosen rescaling exponents. A finite-size analysis of the same data is displayed in part (b) of the figure. The values of $\Delta \ln M/\Delta \ln r_g$ are plotted as functions of $1/M^a$, where $a=0.8$ for NIP and $a=0.6$ for TIP. The straight lines are fits to the data in the range $[0,\ldots,0.05]$. The intersect with the abscissa is the fractal dimension which from these plots equals $d_f=1.899\pm 0.003$ for NIP and $d_f=1.831\pm 0.003$ for TIP.

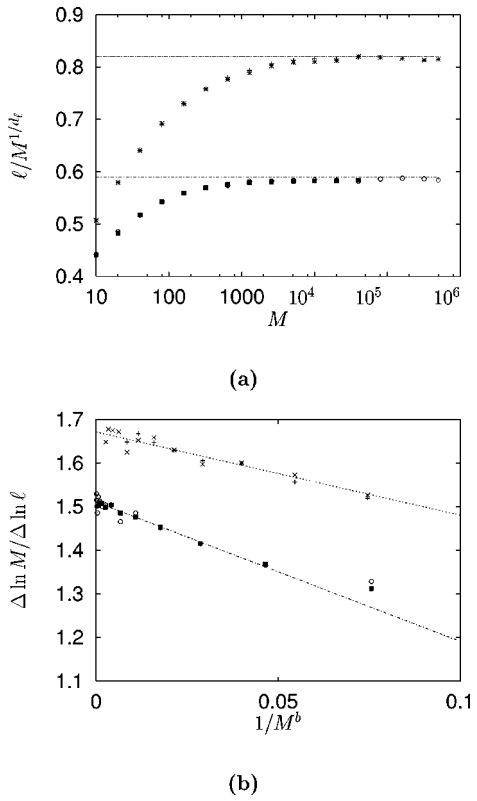

FIG. 3. (a) Plot of the average chemical distance l divided by M^{1/d_l} with $d_l=1.671$ (NIP) and $d_l=1.510$ (TIP) vs the cluster mass. The symbols and the statistical ensembles correspond to those in Fig. 2. For large M, the curves approach a constant value, indicating that the dimension d_l is very close to the chosen rescaling exponents. A finite-size analysis of our data is displayed in part (b) of the figure. The values of $\Delta \ln M/\Delta \ln l$ are plotted as functions of $1/M^b$, where $b=0.45$ for NIP and $b=0.7$ for TIP. The straight lines are fits to the data in the range $[0,\ldots,0.02]$. The intersect with the abscissa is the fractal dimension which from these plots equals $d_l=1.671\pm 0.006$ for NIP and $d_l=1.510\pm 0.005$ for TIP.

different growth steps, characterized by the same logarithmically increasing cluster masses as in the preceding section. For each stage, we determine the chemical distance l of all cluster sites to the site closest to the center of mass. We find the value $\langle l\rangle$ by averaging over all the sites in one cluster over different realizations of the cluster.

The asymptotic scaling behavior of $M\sim\langle l\rangle^{d_l}$ defines the chemical dimension d_l of the cluster. In the same fashion as for the determination of the fractal dimension in the preceding section, we plot $\langle l\rangle/M^{1/d_l}$ vs M for NIP and TIP in Fig. 3(a). As in the case of r_g, here also slight finite-size effects are present at the largest M value, because some very elongated ''linear'' clusters with span larger than $L=3300$ are not sampled. As in the preceding section, we see no significant effect on our analysis.

Since the chemical dimension d_l corresponds to the asymptotic slope of the log-log plot of $\langle l\rangle$ vs M, we find the local slopes $\Delta \ln M/\Delta \ln\langle l\rangle$ and plot them in Fig. 3(b) as a function of M^{-b}. The values of $b=0.45\pm 0.15$ for NIP and 0.70 ± 0.15 for TIP differ from the correction exponents a of the asymptotic behavior of r_g.

Performing a straight line fit, we find the chemical dimension from the extrapolation $M\to\infty$ to be $d_l=1.671\pm 0.006$ for NIP and $d_l=1.510\pm 0.005$ for TIP. The error bars account for the statistical errors and allow for systematic errors in b (estimated by performing fits for different data ranges of M and values of b). Thus, the chemical dimension of TIP turns out to be significantly lower than that of NIP. As in the case of the fractal dimension of TIP, this is caused by the presence of trapped regions in which no further growth occurs (see the next section).

B. Shortest path

The scaling of the length of the shortest path with the Euclidean distance between two sites is $l\sim r^{d_{\min}}$, which defines the shortest path exponent $d_{\min}$ and is reflected in the scaling of the average $\langle l\rangle$ as a function of r_g. We have therefore plotted $\langle l\rangle$ vs r_g for different values of the mass M. Figure 4 displays our data for the NIP and the TIP models. Just as in the previous cases we rescale our data by dividing by known (or tentative values) of $d_{\min}$. For NIP we use

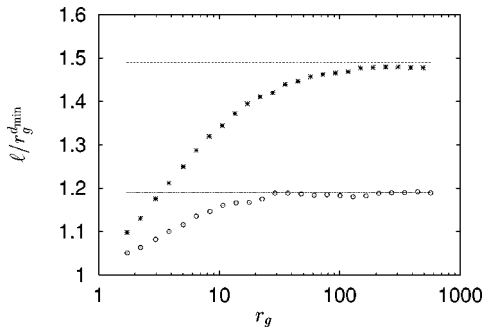

FIG. 4. Plot of $l/r_g^{d_{\min}}$, where $d_{\min}=d_f/d_l$ vs r_g both for NIP ($\bigcirc$) and TIP (*), using interpolated data from the measurement of l and r_g vs M. The fractal and topological dimensions are equal to the values in the preceding figures and yield $d_{\min}=1.133\pm0.005$ for NIP and 1.213 ± 0.005 for TIP.

$d_{\min}=1.133$, which is about 1.5 standard deviations larger, but probably still consistent with the best known value for regular percolation of $d_{\min}=1.130\pm0.002$ reported in [17].

For TIP we use a value of 1.213. We find that the plot reacts rather sensitively to the exact value of $d_{\min}$ and we estimate the error to be about 0.005. The horizontal solid lines have been added as guides to the eye.

We have verified these values of $d_{\min}$ also by measurements of l vs r in ensembles of configurations grown up to a *fixed span L*, without restrictions on the cluster mass. In these ''static'' measurements we have recorded the average value of l and the average minimum value of l for the cluster sites at distance r from the center of mass. These measurements are consistent with the above values, but they are affected by large systematic finite-size effects. In particular, the average $\langle l(r)\rangle$ at distance r displays approximate logarithmic dependence on L, which we will address in detail later (Sec. IV C).

In fact, one can imagine growing a NIP and a TIP cluster on a substrate with the same disorder. The clusters will be exactly equal up to the moment when the first trapped growth sites appear. This is the reason that the accessible perimeter [18] exponents of NIP and TIP are the same [6,19] and thus both very likely equal to $\frac{4}{3}$ [19]. Then, NIP will continue to grow in the ''trapped'' region while TIP cannot grow there any further. Thus, in NIP additional connections will be present which tend to lower the average chemical distance at fixed Euclidean distance. Consequently, the chemical distances in NIP must be shorter than in TIP, resulting in NIP's lower $d_{\min}$.

It is clear that only two of the three quantities d_f, d_l, and $d_{\min}$ are independent, because, for instance, by combining of $M\sim r_g^{d_f}$ and $M\sim l^{d_l}$ one obtains that $l\sim r_g^{d_f/d_l}$ and thus $d_{\min}=d_f/d_l$. This equality is satisfied for our results within the limits given by the error bars, although the result for NIP points to a slightly larger value of $d_l\approx1.673$ compared to the value 1.671 reported in the preceding section.

IV. DISTRIBUTIONS

A. Joint distribution of l and r

A possible step beyond the above scaling analysis is to consider the joint distribution $N_L(l,r)$, where $N_L(l,r)dldr$ is the number of sites with l in the interval $l\cdots l+dl$ and simultaneously r in $r\cdots r+dr$ for clusters of span L. It is our goal to establish scaling properties and, if possible, a functional form of this distribution, as has been outlined and motivated in the Introduction.

To this end we make the commonly used assumption that N_L may be written in the scaling form

$$N(l,r)\sim r^{\alpha}f(l/r^{\beta}), \tag{1}$$

where we have suppressed the dependence on L to indicate that we are interested only in the asymptotic behavior $L\to\infty$. Since $l\sim r^{d_{\min}}$, we expect that $\beta=d_{\min}$. An integration over l yields the radial density $N(r)$ of sites at distance r,

$$N(r)\sim r^{\alpha}\int_0^{\infty}dl\,f(l/r^{d_{\min}}) \tag{2}$$

$$=r^{\alpha}\int_0^{\infty}dx\,r^{d_{\min}}f(x) \tag{3}$$

$$\sim r^{\alpha+d_{\min}}. \tag{4}$$

Since the number $N(r)$ of sites in a (fractal or Euclidean) radial shell of radius r is asymptotically proportional to r^{d_f-1}, we find by comparison that α satifies the relation $\alpha=d_f-1-d_{\min}$. Knowing α and β, we are in a position to extract the scaling function $f(x)$ from our simulations by plotting $N(l,r)/r^{d_f-1-d_{\min}}$ as a function of $l/r^{d_{\min}}$. Figures 5 and 6 show the resulting data collapse both for the NIP and the TIP model. In these plots, we consider r as a parameter and l as a variable, so that different curves correspond to different values of r.

The data that have not collapsed onto the master curve correspond to large values of r, where the finiteness of the system limits the range of l values severely when compared to $r^{d_{\min}}$. Consequently, our assumption (1) breaks down because it has only asymptotical validity.

We like to note here that a second, equivalent scaling form for $N(l,r)$ can be written in analogy to Eq. (1), but with interchanged roles of l and r,

$$N(l,r)\sim l^{\tilde{\alpha}}\tilde{f}(r/l^{\tilde{\beta}}). \tag{5}$$

As above, since $l\sim r^{d_{\min}}$, we have $\tilde{\beta}=1/d_{\min}$. Similarly, by integration of $N(l,r)$ with respect to r, we find the number of sites in the chemical shell l, $N(l)\sim l^{d_l-1}$. We omit the details of the computation here, but simply state the result, $\tilde{\alpha}=d_l-1-1/d_{\min}$. Moreover, the two scaling functions are related by

$$f(x)=x^{-d_l+1+1/d_{\min}}\tilde{f}(x^{-1/d_{\min}}). \tag{6}$$

The above formulas can be used to easily switch between the two representations or to calculate scaling exponents, when $f(x)$ and $\tilde{f}(x^{-1/d_{\min}})$ display singular behavior.

B. Functional form of the scaling function

In Figs. 5(a) and 5(b) we also observe that the scaling function $f(x)$ has a long power-law tail $f(x)\sim x^{-h}$. By com-

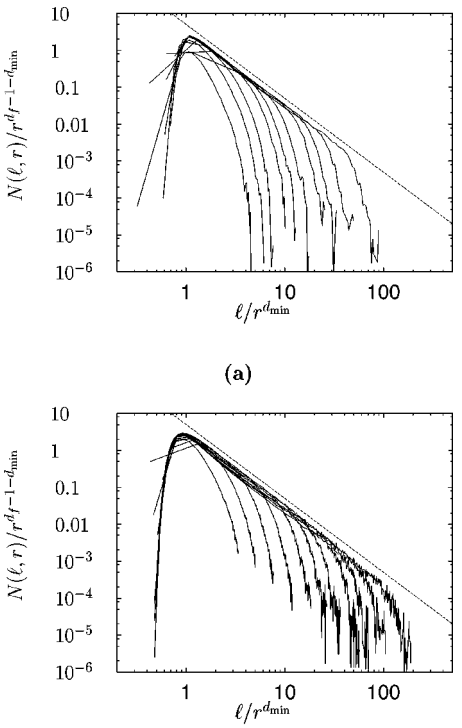

FIG. 5. Data collapse for (a) NIP and (b) TIP of the scaled joint distribution function $N(l,r)/r^{d_f-1-d_{\min}}$ vs $l/r^{d_{\min}}$. The data are averaged over 25 000 (NIP) and 50 000 (TIP) systems of $M=40\,000$. The curve parameter is (right to left) $r=15,25,35,45,65,85,105,145,185,245$ (NIP) and $r=7.5,12.5,17.5,22.5,32.5,42.5,57.5,82.5,117.5,167.5,232.5$ (TIP).

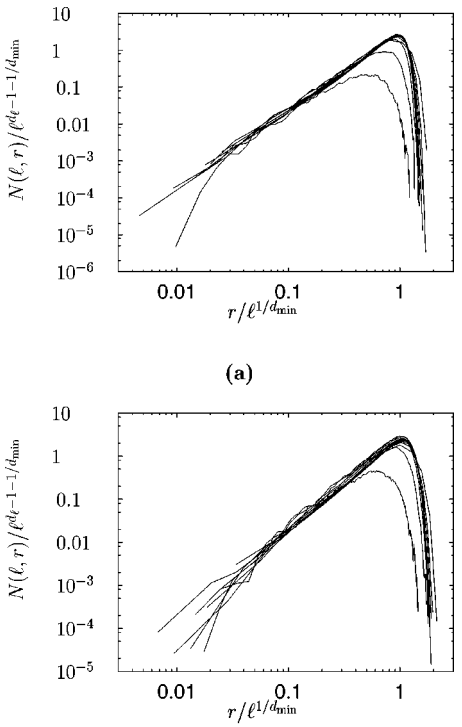

FIG. 6. Data collapse for (a) NIP and (b) TIP of the scaled joint distribution function $N(l,r)/l^{d_l-1-1/d_{\min}}$ vs $r/l^{1/d_{\min}}$. The data are averaged over (NIP) 5050 and (TIP) 5750 systems of $M=500\,000$. The curve parameter is (top to bottom) $l=75,125,175,275,425,625,875,1325,1975,2975,4425$ (NIP) and $l=75,125,175,275,425,625,875,1325,1975,2975,4425,6675$ (TIP).

parison to the solid line with a slope of -2 we see that the characteristic exponent is very close to $h=2.0\pm0.02$ both for NIP and TIP. The value of the exponent $h=2$ is thus independent of the specific percolation model.

Insight into the reasons why $h=2$ has been gained in previous work [11,20] has focused on the conditional probability $\Phi(r|l)$ [8,21] to find a value of r within a fixed chemical shell l. The normalization of $\Phi(r|l)$ is such that it can be interpreted as a regular density in space of sites with characteristic chemical shell number l, i.e.,

$$\int_0^\infty dr r^{d-1}P(r|l)=\text{const.} \tag{7}$$

The constant depends on the spatial dimension but not on l and is, e.g., equal to $1/2\pi$ in 2D. The functional form of $P(r|l)$ is accepted to be of the scaling form [8]

$$P(r|l)\sim\frac{1}{l^{d/d_{\min}}}g\left(\frac{r}{l^{1/d_{\min}}}\right), \tag{8}$$

where

$$g(x)\sim\begin{cases}x^{g_1}, & x\ll 1,\\ x^{g_2}\exp[-ax^\delta], \quad \delta=\dfrac{d_{\min}}{d_{\min}-1}, & x\gg 1.\end{cases} \tag{9}$$

To find the exponent g_1, Ref. [11] has applied an argument originally used by de Gennes for self-avoiding walks [10] to Leath percolation with the result $g_1=d_f+d_{\min}-d$. However, Leath percolation grows one chemical shell after the other and is thus topologically different from NIP such that it is not *a priori* clear that g_1 is the same as in NIP. Since TIP's d_f appears to differ from NIP's, at least in 2D, the validity of this equation for TIP would be surprising.

Let us try to find the value of g_1 from the scaling relations for the distributions. If we integrate $N(l,r)$ over r, we find the number of sites in shell l,

$$N(l)=\int_0^\infty dr N(l,r)\sim l^{d_l-1}. \tag{10}$$

Since Eqs. (7) and (10) are valid for all l, we obtain that $N(r,l)$ and $P(r|l)$ are related by

$$N(l,r)\sim l^{d_l-1}r^{d-1}P(r|l). \tag{11}$$

We now use the expression (8) for $P(r|l)$ to write

$$N(l,r)\sim l^{d_l-1}r^{d-1}l^{-d/d_{\min}}g\left(\frac{r}{l^{1/d_{\min}}}\right). \tag{12}$$

If we rearrange factors of l and r, we can compare this expression with the scaling form (1) for $N(l,r)$,

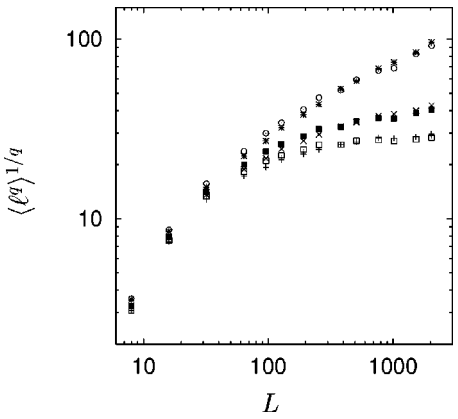

FIG. 7. Generalized averages $\langle l^q(r<10)\rangle^{1/q}$ of 9100 NIP (+,×,*) and TIP systems (□,■,○) plotted vs their linear span L. Different pairs of curves correspond to different $q=0.75,1,1.5$ showing convergence (bottom), nearly logarithmic (center), and power-law divergence (top).

$$N(l,r)\sim r^{d-1}l^{-1/d_{\min}(d-d_f+d_{\min})}g\left(\frac{r}{l^{1/d_{\min}}}\right) \tag{13}$$

$$=r^{d_f-1-d_{\min}}\left(\frac{r}{l^{1/d_{\min}}}\right)^{d-d_f+d_{\min}}g\left(\frac{r}{l^{1/d_{\min}}}\right) \tag{14}$$

$$=r^{d_f-1-d_{\min}}\left(\frac{l}{r^{d_{\min}}}\right)^{(-1/d_{\min})(d-d_f+d_{\min})}g\left(\left(\frac{l}{r^{d_{\min}}}\right)^{-1/d_{\min}}\right), \tag{15}$$

and find how $f(x)$ must be expressed in terms of $g(x)$:

$$f(x)=x^{-d/d_{\min}-1+d_l}g(x^{-1/d_{\min}}). \tag{16}$$

Now we expand this relation for large x such that we can use the asymptotic forms for both $g(x^{(-1/d_{\min})})$ and $f(x)$. One obtains

$$x^{-h}=x^{-d/d_{\min}-1+d_l}x^{-g_1/d_{\min}}. \tag{17}$$

Here we read off that the different exponents are not independent, but that h and g_1 satisfy the equation

$$h=(g_1+d)/d_{\min}+1-d_l, \tag{18}$$

or, conversely, expressing g_1 in terms of h,

$$g_1=(h-1)d_{\min}+d_f-d, \tag{19}$$

where we have applied the identity $d_{\min}=d_f/d_l$. Thus, our numerical finding that $h=2$ implies $g_1=d_f+d_{\min}-d$, for both NIP and TIP, supporting the arguments in Ref. [11] for Leath percolation. Although it is not very surprising that the formula holds both for NIP and Leath percolation—since both are conjectured to be in the same universality class—the possibility that it also holds for TIP suggests a more general validity.

C. Behavior of moments

Specific moments of the distributions discussed above have important physical meaning in applications. For instance, if we fix $r=0$ and consider the average $\langle l(r=0)\rangle$, we obtain the mean chemical length of the paths returning to the origin, which gives some insight into transport properties of systems that can be described by NIP or TIP models. Higher moments of $N(l,r)$ tell us about the fluctuations that have to be expected in transport phenomena—say, the distribution of times that it takes water injected at one oil borehole to reach a second borehole at distance r.

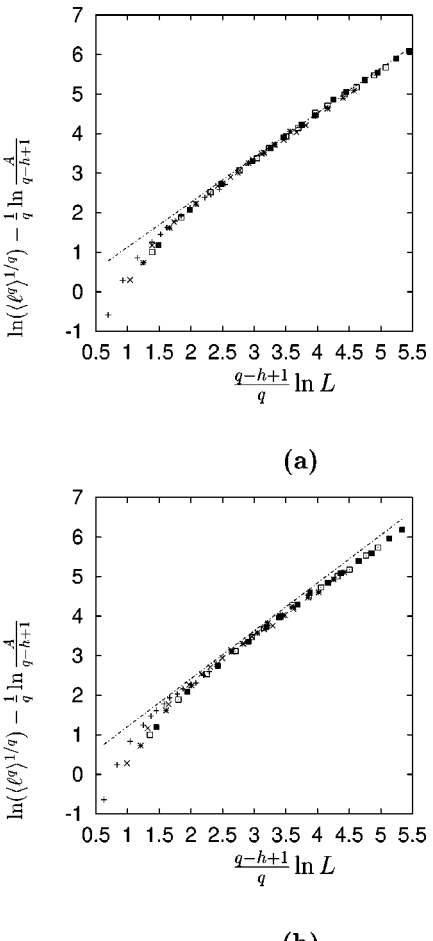

FIG. 8. Scaling plots of $\ln(\langle l(r<10)^q\rangle^{1/q})-(1/q)\ln(A/q-h+1)$ vs $(q-h+1/q)\ln L$ for 9100 NIP (a) and TIP (b) clusters of linear span up to $L=2048$. Different symbols correspond to different $q=1.5(+),2.0(\times),2.5(*),3.5(\square),3.5(\blacksquare)$. From Eq. (23) we expect for $q>h-1$ asymptotically straight lines with slope $d_{\min}$. For comparison, the solid lines indicate these values for the respective case. For TIP, the asymptotic slope appears to be slightly smaller than the value expected from $d_{\min}$, which could be due to finite-size effects. The values of A and h are chosen such that the best possible collapse results: $A=8.0$, $h=2.0$ for NIP, $A=8.0$, $h=2.05$ for TIP.

The value $h=2$ indicates that the distribution of l for fixed r has a Lorentzian tail. The well-known fact that such a distribution does not have a well defined average implies interesting properties for the averages $\langle l(r)\rangle$ or, more generally, for $\langle l(r)^q\rangle^{1/q}$, where we take the moment q as a positive real parameter.

Let us consider ensembles of clusters grown up to fixed span L. Typically, in such clusters, the longest chemical path has length $L^{d_{\min}}$. When we now use the scaling form for $N(r,l)$ to compute $\langle l(r)^q\rangle$, we will extend the integrals to

TABLE I. Summary of the various exponent values in NIP, regular 2D percolation, and TIP.

	d_f	d_l	$d_{\min}$	h	a	b
2D NIP	1.899 ± 0.003	1.671 ± 0.006	1.133 ± 0.005	2.00 ± 0.10	0.80 ± 0.15	0.45 ± 0.15
2D percolation	91/48	1.678 ± 0.003	1.130 ± 0.002 [17]	2.0 [11]		
2D TIP	1.831 ± 0.003	1.510 ± 0.005	1.213 ± 0.005	2.05 ± 0.10	0.60 ± 0.15	0.70 ± 0.15

$L^{d_{\min}}$, which introduces effectively a cutoff function multiplying $N(r,l)$,

$$\langle l(r)^q\rangle = \int_1^{L^{d_{\min}}} dl\, l^q N(r,l). \tag{20}$$

If L is sufficiently large, then the integral will be dominated by the tail contributions and $f(l), l \gg 1$ will be close to its asymptotic form $\sim A l^{-h}$, with A being the constant of proportionality. We will concentrate on the case that r is a small positive constant, say 1. Then, for sufficiently large L the relation

$$\langle l^q(1)\rangle \approx A \int_1^{L^{d_{\min}}} dl\, l^q l^{-h} \tag{21}$$

holds. For $q = h-1$, the integral diverges logarithmically, for $q > h-1$ in a power-law fashion, but for $q < h-1$ the integral converges to a constant independent of L. In summary, we obtain for $\langle l(1)^q\rangle^{1/q}$

$$\langle l^q(1)\rangle^{1/q} \approx \begin{cases} \text{const}, & q < h-1, \\ [A d_{\min} \ln(L)]^{1/q}, & q = h-1, \\ A\left(\dfrac{A}{q-h+1}\right)^{1/q} L^{d_{\min}(q-h+1/q)}, & q > h-1. \end{cases} \tag{22}$$

Since $h=2$, we expect that the regular average $\langle l(1)\rangle$ for $q = h-1 = 1$ diverges logarithmically. Averages derived from smaller moments become independent of L and those for larger moments diverge as powers of L. These predictions are supported by the simulation as shown in Fig. 7, where we display $\langle l^q(1)\rangle^{1/q}$ as a function of cluster size for $q = 0.75, 1, 1.5$ both for NIP and TIP. The abscissa scale is logarithmic, so that the two central curves for $q=1$ should be linear for large L. We see clearly the convergence for the moments below $q=1$ and the divergence for larger moments.

If we plot the logarithm of the diverging generalized averages $\ln(\langle l(1)^q\rangle^{1/q})$, we expect asymptotically

$$\ln(\langle l(1)^q\rangle^{1/q}) \approx \frac{1}{q}\ln\left(\frac{A}{q-h+1}\right) + d_{\min}\frac{q-h+1}{q}\ln L. \tag{23}$$

Thus, plotting $\ln(\langle l(1)^q\rangle^{1/q}) - (1/q)\ln(A/q - h + 1)$ vs $(q - h + 1/q)\ln L$ as an independent variable on the abscissa, the graph becomes a straight line with slope $d_{\min}$. Such a plot constitutes an independent way to determine h and $d_{\min}$. We find the value of h by demanding that the graph should be straight for large L and determine $d_{\min}$ from its slope.

Our data for NIP [Fig. 8(a)] support nicely $h \simeq 2$ and $d_{\min} = 1.133$ as shown in Fig. 8(a).

The TIP data [Fig. 8(b)], however, are slightly less convincing. We obtain the best straight line for $h = 2.05$, but h has only a precision of 0.1. Likewise, the corresponding asymptotic slope is about 1.18, smaller than the expected value of $d_{\min} = 1.213$, which is indicated by the straight line added in the figure.

V. DISCUSSION AND SUMMARY

In this paper we have studied, along with the fractal dimension d_f, several structural exponents of NIP and TIP, which are summarized in Table I. We find strong evidence that NIP and TIP in 2D fall into different universality classes: we find that d_f for the two models differs by more then about 20 standard deviations. In addition, the shortest path exponent in TIP is larger than for NIP by about 16 standard deviations, reflecting the additional constraints imposed on the topology by the trapped regions in the TIP interior. Consequently, the chemical dimension of NIP is larger than that of TIP. However, all measured structural exponents of NIP are within the error bars equal to those of regular percolation, thus providing convincing numerical evidence for the conjecture that NIP and regular percolation fall into the same universality class.

We have also studied the distribution $N(l,r)$ of the number of cluster sites with chemical distance l and Euclidean distance r from the cluster center. We find a scaling form of $N(r,l) \sim r^{d_f - 1 - d_{\min}} f(l/r^{d_{\min}})$, with the interesting property that $f(x) \sim x^{-2}$ for large x, *independent* of the model (NIP or TIP). The very large exponent of (-2) gives rise to a logarithmic behavior with system size, if average values of l are calculated as functions of r, more generally all qth-order moments $\langle l^q\rangle$ of $N(l,r)$ will diverge with system size for $q \geqslant 1$ and converge for $q < 1$.

ACKNOWLEDGMENTS

We kindly acknowledge financial support by the German Israeli Foundation (GIF) and benefits from computational resources at the Institut for Computer Applications, Universität Stuttgart, Germany. S.S. is grateful to the scientific council of NATO for financial aid (granted through the DAAD, Bonn).

[1] D. Wilkinson and J. F. Willemsen, J. Phys. A **16**, 3365 (1983).
[2] C. P. Stark, Nature (London) **352**, 423 (1991).
[3] P. Bak, C. Tang, and K. Wiesenfeld, Phys. Rev. Lett. **59**, 381 (1987).
[4] R. Chandler, J. Koplik, K. Lerman, and J. Willemsen, J. Fluid Mech. **119**, 249 (1982).
[5] L. Furuberg, J. Feder, A. Aharony, and T. Jøssang, Phys. Rev. Lett. **61**, 2117 (1988).
[6] P. Meakin, Physica A **173**, 305 (1991).
[7] M. Porto, S. Havlin, S. Schwarzer, and A. Bunde, Phys. Rev. Lett. **79**, 4060 (1997).
[8] S. Havlin and D. Ben-Avraham, Adv. Phys. **36**, 695 (1987).
[9] N. V. Dokholyan, Y. Lee, S. V. Buldyrev, S. Havlin, H. E. Stanley, and P. King, J. Stat. Phys. (to be published); P. King *et al.*, Physica A (to be published).
[10] P. G. de Gennes, *Scaling Concepts in Polymer Physics* (Cornell University Press, Ithaca, 1979).
[11] M. Porto, S. Havlin, H. E. Roman, and A. Bunde, Phys. Rev. E **58**, 5205 (1998).
[12] Our NIP algorithm maintains a list of the (active) perimeter growth sites of the cluster using a binary tree structure that allows us to find the site with the largest random number in $O(1)$ time and to insert new perimeter sites in $O(\ln N)$ time. Thus, we can grow NIP clusters with $O(N\ln N)$ effort, typically about 20 000 sites per second (DEC ALPHA 255/233 workstations).
[13] To implement the trapping condition, we check whether the most recently added site has at least two next nearest neighbors, so that growth sites could have been trapped in the cluster interior. If so, oriented walks (at most three) are started on the just added site, pointing away from it to the neighboring *empty* sites (i.e., neither cluster nor growth sites). The walks continue until all but one of them have again reached the site of origin. The growth sites visited by these walks are then eliminated from the list of active sites. This latter technique has been suggested in Ref. [6] and we use it here in conjunction with the tree structure to maintain our list of active sites. Although due to the accessibility constraint the resulting algorithm scales less favorably than the NIP technique, clusters with $M=500\,000$ need about $250s$ to grow.
[14] A. Aharony, in *Directions in Condensed Matter Physics*, edited by G. Grinstein and G. Mazenko (World Scientific, Singapore, 1986), Chap. 1.
[15] D. Stauffer and A. Aharony, *Introduction to Percolation Theory*, 2nd ed. (Taylor & Francis, London, 1992).
[16] We have also performed a ''sandbox'' measurement of the fractal dimension. To this end we grow clusters up to span L, and then counting the number $M(r)$ of cluster sites within circles of radius r. In a plot of $\ln M(r)$ vs $\ln r$ for NIP and TIP, we find a slope equaling d_f within the error bars. However, the results of the sandbox method are affected by pronounced finite-size effects, which are more difficult to control than those in the constant M ensembles.
[17] H. J. Herrmann and H. E. Stanley, J. Phys. A **21**, L829 (1988).
[18] T. Grossman and A. Aharony, J. Phys. A **19**, L745 (1986); **20**, L1193 (1987).
[19] S. Schwarzer, S. Havlin, and H. E. Stanley, Phys. Rev. E **49**, 1182 (1994).
[20] *Fractals and Disordered Systems*, 2nd ed., edited by A. Bunde and S. Havlin (Springer, New York, 1996).
[21] A. U. Neumann and S. Havlin, J. Stat. Phys. **52**, 203 (1988).